

## Inversion of the COPROD2 Data by a Method of Modelling

A. K. AGARWAL and J. T. WEAVER

*Department of Physics & Astronomy and School of Earth & Ocean Sciences,  
University of Victoria, Victoria, B.C., Canada, V8W 3P6*

(Received March 9, 1993; Revised August 5, 1993; Accepted September 1, 1993)

Separate inversions of the North American Central Plains (NACP) and Thompson Belt (TOBE) anomalies are undertaken using a method in which a ‘least-blocked’ model is sought. The algorithm first constructs a 3-column starting model by the juxtaposition of 1D ‘least-layered’ inversions of the TE data at 3 sites covering the region under investigation and then minimizes the least squares fit of the TE and TM apparent resistivity and phase responses by adjusting the positions of the horizontal and vertical boundaries and the resistivities of the resulting blocks in the composite starting model. The procedure is repeated with successively 4, 5, ... columns until the addition of further columns is no longer justified by a significant improvement in the fit. Inversion of the COPROD2 data by this method reveals a conductive surface layer of sediments slightly less than 3 km thick across the whole region, underlain by an NACP anomaly roughly 120 km wide and composed of two adjoining conductive blocks extending to the basement 60 km deep and whose top surfaces are at depths of roughly 12 km and 19 km respectively, and a TOBE anomaly consisting of a single narrow block only about 7 km wide rising from the basement to the base of the surface sedimentary layer. The TOBE anomaly is found to be much more conductive than the NACP anomaly.

### 1. The Modelling Method

The method of modelling used in this paper to invert the COPROD2 data involves a straightforward optimization of a series of starting models with successively 3, 4, 5, ... columns compiled from one-dimensional ‘least-layered’ inversions (WEAVER and AGARWAL, 1993) of TE data at 3, 4, 5, ... selected sites along the profile. The procedure continues until the addition of extra columns is no longer justified by a significant improvement in the fit of the magnetotelluric responses (apparent resistivity  $\rho_a$  and phase  $\phi$ ) to the real data as determined by application of a statistical  $F$ -test. Thus the final model obtained is formed from the minimum number of columns justified by the data with each column being ‘least-layered’ in the sense of WEAVER and AGARWAL (1993). It is therefore called the ‘least-blocked’ model.

The method represents a generalization to two dimensions of the strategy underlying the automatic one-dimensional scheme which itself was based on the philosophy expressed by FISCHER and LEQUANG (1981) that the best-fitting model with the fewest number of layers should be sought. There are added complications, however, because in two dimensions both the TE and TM apparent resistivity and phase responses are fitted with the data at all sites along the array, and not only resistivities and horizontal layer boundaries but also the positions of the vertical boundaries of the columns are available for adjustment during optimization. The method is very demanding on computing time; an efficient two-dimensional modelling program with a fully automatic grid generator and access to a powerful workstation dedicated to this single task are essential prerequisites to its successful implementation.

Suppose that the TE and TM responses are to be fitted at  $N$  periods  $T_n$  ( $n = 1, 2, \dots, N$ ) and  $K$  sites  $y = y_k$  ( $k = 1, 2, \dots, K$ ). Then the optimized fit in the least squares sense is obtained

by minimizing the variance of fit  $s_\nu^2$  (BEVINGTON, 1969, p. 187) where

$$s_\nu^2 = (\epsilon_{TE}^2 + \epsilon_{TM}^2 + \eta_{TE}^2 + \eta_{TM}^2)/\nu, \tag{1}$$

$$\epsilon^2 = \sum_{k=1}^K \sum_{n=1}^N W_{k,n} \left[ \frac{1}{2} \ln \left( \rho_a(y_k, T_n) / \rho_a^{(c)}(y_k, T_n) \right) \right]^2, \tag{2}$$

$$\eta^2 = \sum_{k=1}^K \sum_{n=1}^N w_{k,n} [\phi(y_k, T_n) - \phi^{(c)}(y_k, T_n)]^2 \tag{3}$$

with  $\nu = 4KN - p$  representing the number of degrees of freedom, i.e. the total number of data points to be fitted less the number  $p$  of model parameters available for adjustment during optimization. Subscripts TE or TM are attached to  $\epsilon$ ,  $\eta$ ,  $\rho_a$ ,  $\phi$  and the weighting functions  $W$  and  $w$ , to indicate the polarization of the field to which they refer, while the superscript  $(c)$  on  $\rho_a$  and  $\phi$  refers to the calculated response of the model rather than the observation. The weighting functions  $W$  and  $w$  are defined as the normalized inverses of the variances of the data errors in  $\frac{1}{2} \ln \rho_a$  and  $\phi$  which are assumed to be independent and normally distributed about the true response, i.e.

$$W_{k,n} = \left( \bar{\sigma}^{(\rho)} / \sigma_{k,n}^{(\rho)} \right)^2, \quad w_{k,n} = \left( \bar{\sigma}^{(\phi)} / \sigma_{k,n}^{(\phi)} \right)^2 \tag{4}$$

where  $\sigma_{k,n}^2$  is the variance (of  $\frac{1}{2} \ln \rho_a$  or  $\phi$  according to the attached superscript) for period  $T_n$  at site  $y_k$ , and

$$\bar{\sigma}^2 = \frac{1}{(1/KN) \sum_{k=1}^K \sum_{n=1}^N (1/\sigma_{k,n}^2)} \tag{5}$$

with appropriate superscripts  $\rho$  or  $\phi$  on  $\sigma$ , is the reciprocal of the mean of the inverse variances. Assuming that the error bounds supplied with the COPROD2 data are twice the standard error in length, the square roots of the variances are given in terms of the bounding values  $\rho_a^{\max}$ ,  $\rho_a^{\min}$  and  $\phi^{\max}$ ,  $\phi^{\min}$ , by

$$2\sigma_{k,n}^{(\rho)} = \frac{1}{2} \kappa \ln(\rho_a^{\max} / \rho_a^{\min}), \quad 2\sigma_{k,n}^{(\phi)} = \kappa(\phi^{\max} - \phi^{\min}) \tag{6}$$

where  $\kappa$  is a factor which determines what is meant by ‘standard error’. If it means 1 standard deviation then  $\kappa = 1$ ; if it means ‘probable error’ then  $\kappa = 1.48$ . Its precise value is unimportant, however, because it cancels out in subsequent calculations. Henceforth we shall refer to the variance of the fit  $s_\nu^2$  as simply the ‘misfit’ and for simplicity we shall omit the parameter  $\nu$  defining the number of degrees of freedom. Note that if unnormalized weights were used in the definitions of  $\epsilon$  and  $\eta$  in (2) and (3), then (1) would become the familiar reduced chi-square distribution defined by  $\chi_\nu^2 = \chi^2/\nu$  where

$$\chi^2 = \left( \epsilon_{TE} / \bar{\sigma}_{TE}^{(\rho)} \right)^2 + \left( \epsilon_{TM} / \bar{\sigma}_{TM}^{(\rho)} \right)^2 + \left( \eta_{TE} / \bar{\sigma}_{TE}^{(\phi)} \right)^2 + \left( \eta_{TM} / \bar{\sigma}_{TM}^{(\phi)} \right)^2. \tag{7}$$

It is expected that if the model response is a good fit to the data then  $\chi_\nu^2 \approx 1$  (BEVINGTON, 1969, p. 189). Noting that an overly optimistic estimation of the experimental errors could lead to unreliable large values of  $\chi_\nu^2$  (too small a value of  $\sigma^2$  leads to unreasonably large weights  $w$  and  $W$ ), some authors (e.g. PEDERSEN and RASMUSSEN, 1989; DEGROOT-HEDLIN and CONSTABLE, 1990) have suggested enlarging the error bars in some prescribed manner to ensure that  $\chi_\nu^2 \approx 1$  for the best fitting response. For the comparative study presented in this paper, however, we have resisted the temptation to tamper with the data in this manner.

In our modelling procedure, the significance of the improvement in the fit of the model response to the data when more structure (i.e. an additional column) is added to a model with (say)  $\nu_1$  degrees of freedom, is tested by computing

$$F = \frac{\Delta\chi^2/(\nu_1 - \nu_2)}{\chi_{\nu_2}^2} \quad (8)$$

where  $\nu_2$  is the (smaller) number of degrees of freedom of the new (augmented) model and  $\Delta\chi^2$  is the difference of the  $\chi^2$  distributions for the models with  $\nu_1$  and  $\nu_2$  degrees of freedom respectively. This is the well-known  $F$  distribution, being a ratio of reduced  $\chi^2$  distributions with respectively  $\nu_1 - \nu_2$  and  $\nu_2$  degrees of freedom. Its probability distribution is tabulated or can be calculated using library subroutines, and if the probability of  $F$  is found to be less than 5%, then the hypothesis that the value could have been obtained by chance is rejected at the 95% confidence level, whence it is concluded that the additional column led to a significant improvement in the fit. Otherwise the procedure halts on the evidence that additional structure is no longer justified by improvement of fit. (If  $F$  turns out to be negative the new model is automatically rejected since in that case the fit has actually worsened.)

Following SMITH and BOOKER (1988) who tested the 'colour' of the fit in 1D inversions, we have used the Spearman statistic  $D$  to test for systematic bias in the fit of our final model responses. By systematic bias we mean that there has been a tendency for the inversion scheme to minimize the overall misfit by systematically improving the responses at certain particular sites or periods without due regard for the fit at other sites and periods in the data set. While it might be possible to achieve the smallest misfit with this biased approach, a somewhat larger value would be more acceptable if the fit were more evenly spread over the entire range of sites and periods. The Spearman statistic is defined as

$$D = \sum_{i=1}^{NK} (R_i - S_i)^2 \quad (9)$$

where  $R_i$  is the rank of the sum of the squares of the residuals, normalized by their variances, of the fitting parameters  $\frac{1}{2} \ln(\rho_a)_i$  and  $(\phi)_i$  at a certain period and site, and  $S_i$  is the rank of these particular data when responses are ordered successively by periods and then sites. The value of  $D$  and its probability were calculated automatically using published subroutines (PRESS *et al.*, 1989). Let  $P$  be the probability of  $D$  being greater than the value calculated; then if  $P$  is less than .05, it is concluded with 95% confidence that there is a trend present in the data residuals. This test was applied to the residuals in both the TE and the TM data.

## 2. Application of the Inversion Scheme

Unfortunately it was not feasible to investigate both the NACP and TOBE anomalies together because their distance apart was sufficiently great that it would have been impossible to satisfy simultaneously the requirements of a wide numerical grid which encompassed the two anomalies plus a fine mesh that resolved their structure properly, without imposing demands on computer memory and time that are well beyond the resources available. The wide separation of the anomalies does mean, however, that it is probably reasonable to treat them individually as suggested by JONES and CRAVEN (1990) because the mutual coupling between them is almost certainly minimal.

All inversions were carried out on a dedicated IBM RS 6000-320E workstation using a new forward modelling program (written by Helena E. Poll) based on the finite difference method with integral boundary conditions, and incorporating a period-dependent, spatially variable grid

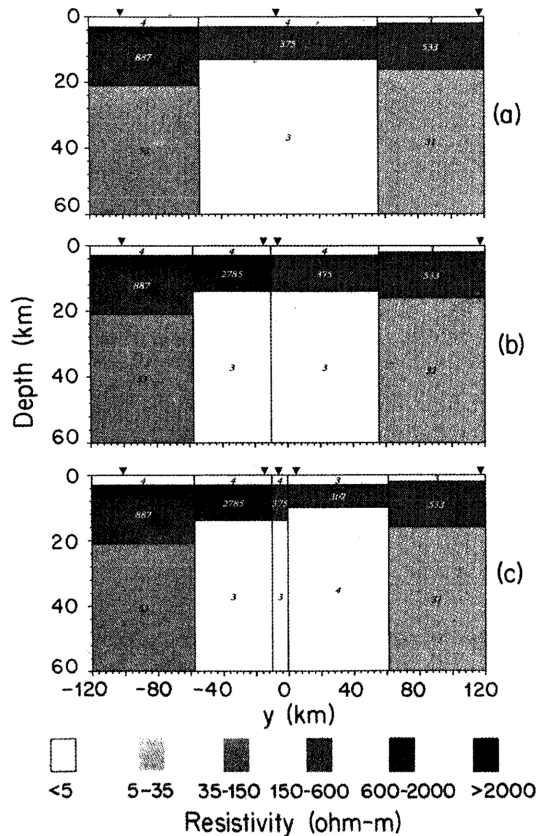


Fig. 1. Starting models for the NACP anomaly: (a) 3 columns, (b) 4 columns and (c) 5 columns. The positions of the sites where the 1D inversions were made are indicated by the inverted black triangles. (After AGARWAL *et al.*, 1993).

which is automatically designed for each submitted model. Misfit minimization was handled by the simple but robust routine MINDEF used by FISCHER and LEQUANG (1981); it is similar in strategy to the ravine search described by BEVINGTON (1969, p. 207). In principle, however, any optimization routine (Marquardt, simplex, quasi-Newton, conjugate gradient etc.) could be substituted in its place.

### 2.1 The NACP anomaly

The COPROD2 data set consists of 40 responses covering the period range  $2.6 \times 10^{-3}$  to 1820 s at each of 35 sites spanning a 407 km traverse. For the NACP anomaly a reduced data set known as COPROD2R is available; it includes the 20 sites whose locations are at  $y = -113.5, -100.9, -93.0, -84.6, -74.4, -64.9, -55.7, -45.8, -35.0, -25.9, -14.6, -5.9, 4.9, 22.8, 41.8, 54.5, 64.2, 79.5, 96.2$  and  $117.3$  km traversing the anomaly, and 4 periods  $T = 85.3, 170.7, 341.3$  and  $682.7$  s. We have supplemented the reduced data set with responses at the 3 shorter periods  $T = 10.7, 21.3$  and  $42.7$  s for fitting the TE and TM responses at the 20 sites along the array, on the assumption that these additional periods will ensure that shallow features are more accurately

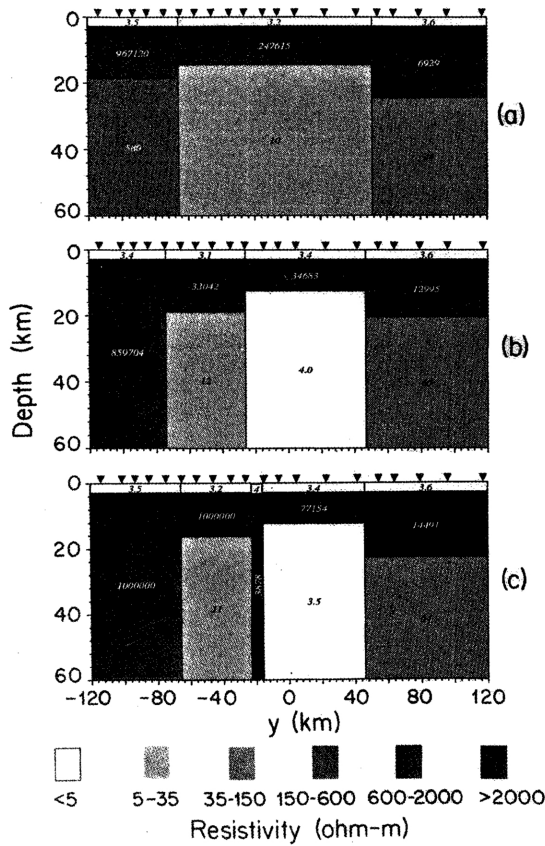


Fig. 2. Final models for the NACP anomaly: (a) 3 columns with misfit  $s^2 = 1.61 \times 10^{-3}$ , (b) 4 columns with misfit  $1.23 \times 10^{-3}$ , and (c) 5 columns with misfit  $1.26 \times 10^{-3}$ . The ‘least-blocked’ model is the 4 column model in (b). The uniform half-space below 60 km has a resistivity of 61  $\Omega\text{m}$ . (After AGARWAL *et al.*, 1993).

resolved. The application of our procedure to the NACP anomaly has already been discussed in detail by AGARWAL *et al.* (1993) and will only be outlined here.

In constructing the 3 column starting model shown in Fig. 1(a) from 1D inversions of the TE data at 3 selected sites, two of the sites were chosen close to the beginning and end of the array at  $-100.9$  km and  $117.3$  km, and the third at  $-5.9$  km somewhere near the middle. Vertical boundaries were drawn at the midpoints between the sites to form the three columns. The middle column of width  $109.1$  km is a 3 layer structure given by 1D inversion, according to the method of WEAVER and AGARWAL (1993), of the TE data at  $y = -5.9$  km while the (infinitely wide) first and third columns are also 3 layer structures given by similar 1D inversions at  $-100.9$  km and  $117.3$  km respectively. The entire model was then terminated at the fixed depth of 60 km by a uniform half-space whose resistivity was initially set equal to the resistivity of the bottom layer in the left-hand column. The number of layers in each column is, of course, already optimized in the sense of the structures being ‘least layered’ models obtained by 1D inversions of the TE data at the 3 sites. In total there were 18 adjustable parameters—the resistivities of the 9 blocks and the underlying half-space, plus the positions of the 2 vertical and 6 horizontal boundaries,

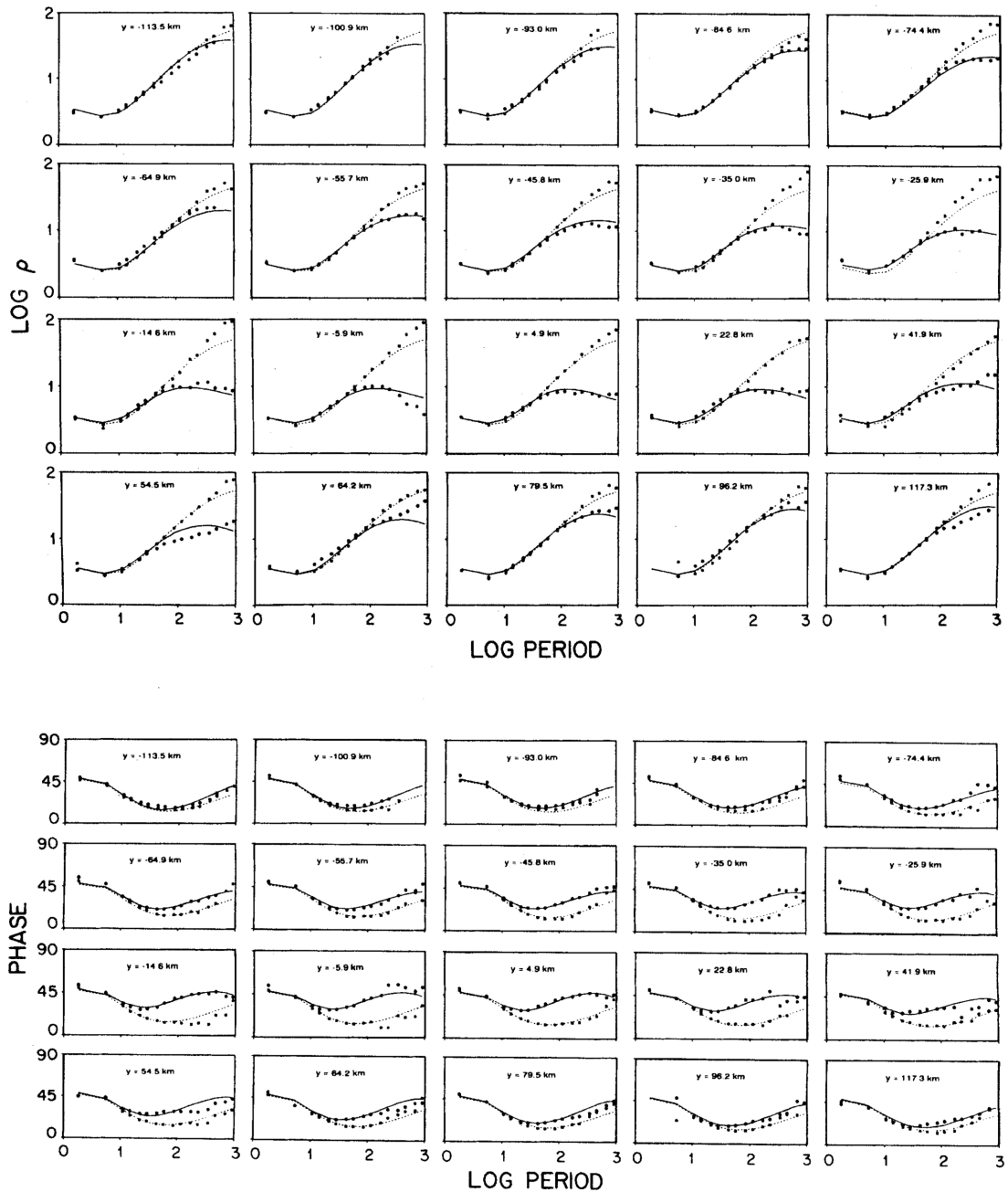


Fig. 3. Magnetotelluric responses at the 20 sites traversing the NACP anomaly—apparent resistivity (top) and phase (bottom). The solid and broken line curves are respectively the TE and TM responses computed for the 4 column ‘least-blocked’ model shown in Fig. 2(b). Observed values taken from the COPROD2 data set are depicted by circles and squares respectively. (After AGARWAL *et al.*, 1993).

or  $560 - 18 = 542$  degrees of freedom  $\nu$ . Optimization with the aid of MINDEF led to the 3 column model in Fig. 2(a) which generated response curves with misfit  $s^2 = 1.61 \times 10^{-3}$  when compared with the COPROD2 data for the 7 periods at all 20 sites. The criterion used to halt the search for a minimum was that the change in misfit between successive trials should be less than 0.01%, or that 2400 calls to MINDEF (including the unsuccessful ones as well as those that led to an advance towards the minimum) should have been executed, whichever occurred first. In general it was observed that when the number of adjustable parameters was 35 or less, the search tended to meander meaninglessly around the minimum with little improvement in misfit after about 500–600 calls to MINDEF. An upper limit of 2400 was therefore considered a very safe cut-off.

Subsequent starting models with 4 and 5 columns, shown in Figs. 1(b) and (c), were compiled by adding new central sites to the existing ones, at  $-14.6$  km and  $4.9$  km respectively. In the 4 column model there are 24 adjustable parameters—13 resistivities including that of the half-space below 60 km, plus 3 vertical and 8 horizontal boundaries—giving  $\nu = 536$ . After minimizing the fit of the TE and TM responses at the 7 periods and all 20 sites, the final model in Fig. 2(b) was obtained with misfit  $s^2 = 1.23 \times 10^{-3}$ , which certainly represents a significant improvement in the fit at the 95% confidence level according to the  $F$ -test. The starting and final 5 column models are similarly depicted in Figs. 1(c) and 2(c). This time the misfit value, with  $\nu = 530$ , was found to be  $s^2 = 1.26 \times 10^{-3}$  indicating a slight deterioration of the fit and therefore automatic rejection of the model. Thus the required 'least-blocked' model is the 4 column model displayed in the grey-scale format of Fig. 2(b) but reproduced in standard colour-coded form in JONES (1993).

In Fig. 3 the TE and TM apparent resistivity and phase responses of the final 4 column model in Fig. 2(b) are compared with the corresponding measured responses at all 20 sites. Note that the comparison has been extended to 16 periods in the COPROD2 data rather than just the 7 used in the optimization. They give a wider and denser coverage of the entire range of periods which better indicates how well the responses of the final model fit the entire data set. The agreement is quite good in general but there are a few exceptions such as the underestimate of the TE apparent resistivity values at long periods at site 64.2 km, and the overestimate of apparent resistivity values at sites  $-5.9$  and  $117.3$  km. There are also long period mismatches in the TM apparent resistivities at the locations  $-113.5$ ,  $-93.0$ ,  $-74.4$ ,  $-35.0$ ,  $-25.9$ ,  $-14.6$ ,  $-5.9$ ,  $4.9$  and  $54.5$  km which are probably associated with the large error bars at long periods because the calculated values, 0.54 and 0.15 respectively, of the probability of the Spearman statistic  $D$  defined in (9), for the fitting of the TE and TM responses gave no indication of any systematic period or site bias. Moreover, a plot of the normalized residuals showed that they were actually smaller at long periods than at short periods where the error bars were very tightly defined.

## 2.2 The TOBE anomaly

The TOBE anomaly was investigated by considering the last 8 of the 35 sites along the MT profile, i.e. those with locations at  $y = 117.3$ ,  $135.3$ ,  $155.2$ ,  $169.4$ ,  $181.2$ ,  $194.1$ ,  $214.6$  and  $232.8$  km, and the same 7 periods used previously. The 3 column starting model shown in Fig. 4(a) was assembled from 1D inversions of the TE apparent resistivity and phase data at sites  $y = 117.3$ ,  $169.4$  and  $214.6$  km near the ends and middle of the array, for the chosen 7 periods. For this model there are 18 adjustable parameters, but with fewer sites than for the NACP anomaly, only 206 degrees of freedom  $\nu$ . The optimized 3 column model in Fig. 5(a) generated response curves with misfit  $s^2 = 2.93 \times 10^{-3}$  when compared with the COPROD2 data for the 7 periods at all 8 sites.

Next the 4 column starting model with  $\nu = 198$  was constructed by including one more site at  $y = 155.2$  km, as shown in Fig. 4(b). Minimizing the misfit yielded the final model in Fig. 5(b) with  $s^2 = 2.12 \times 10^{-3}$ , which is a marked improvement on the 3 column model. Thus the procedure continued with another column added beneath the site positioned at  $y = 181.2$  km.

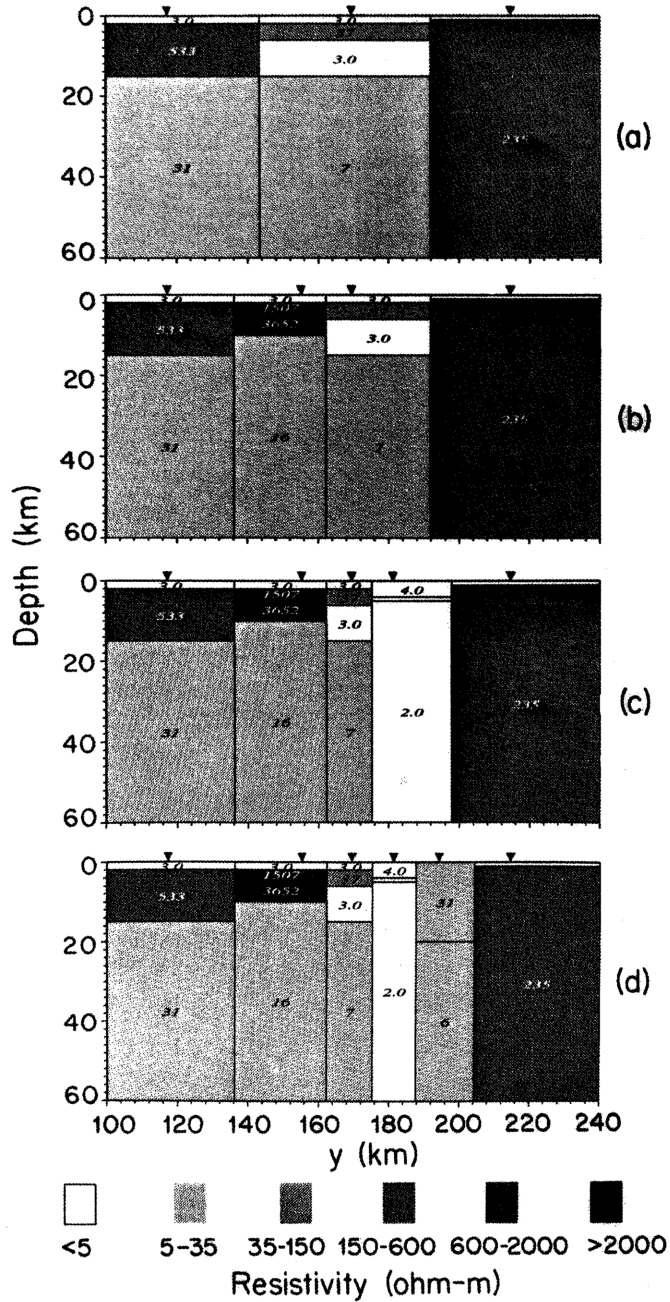


Fig. 4. Starting models for the TOBE anomaly: (a) 3 columns, (b) 4 columns, (c) 5 columns and (d) 6 columns. The positions of the sites where the 1D inversions were made are indicated by the inverted black triangles.

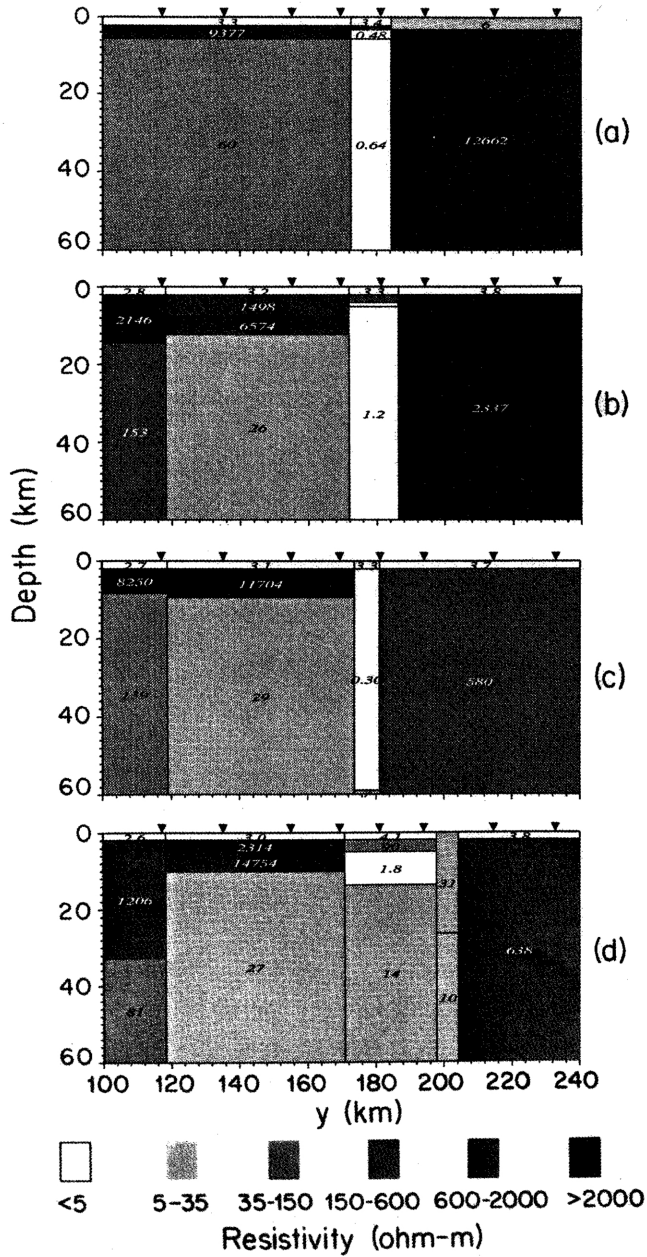


Fig. 5. Final models for the TOBE anomaly corresponding to the starting models (a), (b), (c) and (d) in Fig. 4. The misfit values are respectively  $s^2 = 2.93 \times 10^{-3}$ ,  $2.12 \times 10^{-3}$ ,  $1.82 \times 10^{-3}$  and  $1.07 \times 10^{-2}$ ; the 'least-blocked' model is (c). The uniform half-space below 60 km has a resistivity of 72  $\Omega\text{m}$ .

The new starting model is depicted in Fig. 4(c) and has 32 adjustable parameters with  $\nu = 192$ . The final model in Fig. 5(c) appears to have only 4 rather than 5 columns. This is because the fourth column from the left in the starting model was compressed to only 1 km in width during the minimization process and cannot be reproduced clearly on the diagram. In any case its resistivity structure was such that it blended into the anomaly and exerted virtually no influence on the response curves. It will also be seen that the 4 layer third column has been reduced to 3 layers in the final model. This was a genuine reduction—layers only 1 km thick *can* be shown on the diagram (an example is the bottom layer in the same column) because the aspect ratio permits reproduction of greater detail in the vertical direction—but if the minimization procedure attempts to shrink a layer (or column) to less than 0.5 km in thickness (width) then the boundaries automatically merge while retaining their status as separate parameters in order not to increase the number of degrees of freedom. After all, the layer may be required to open up again in the continuing search for the minimum. (Likewise, the program automatically fixes thicknesses or widths lying between 0.5 km and 1 km at the value of 1 km.) The layer eliminated was the resistive one between the sedimentary cover and the top of the anomaly—a prominent feature in the previous models with fewer columns. The misfit for the model in Fig. 5(c) is  $s^2 = 1.82 \times 10^{-3}$ , which although only a slight improvement on the previous value, was found by an application of the  $F$ -test to be statistically significant at the 95% confidence level. The investigation therefore advanced to the starting model in Fig. 4(d) in which a sixth column has been added beneath the site at  $y = 194.1$  km, thereby reducing the number of degrees of freedom to  $\nu = 188$ . The final model is shown in Fig. 5(d); note that one of the columns, the fourth from the left in Fig. 4(d), has also been excluded from the diagram since it too was only 1 km wide, but this time all 4 layers have been retained in the third column. The extra column had only 2 layers in the starting model and failed to reproduce the surface sedimentary layer. This unlikely feature persisted through to the final model, the lack of layers restricting the possible options for eliminating it either to compressing the entire column to negligible thickness or to raising the only horizontal layer boundary in the column to the shallow depth of the base of the sediments while reducing the resistivity above it to a value consistent with the rest of the surface layer. The program chose not to follow either route in the search for the minimum. Since the misfit of the response increased to  $s^2 = 1.07 \times 10^{-2}$  for this model, it was rejected and the procedure stopped at this point by returning to the structure depicted in Fig. 5(c) as the required 'least-blocked' model. The grey-scale diagram there is supplemented, for comparison purposes, by a full colour illustration elsewhere in this issue.

The apparent resistivity and phase responses of the 'least-blocked' model from Fig. 5(c) are compared with the observed (COPROD2) values in Fig. 6 at the 8 selected sites straddling the TOBE anomaly. In general the agreement is quite good at the 3 sites  $y = 169.4$ , 181.2 and 194.1 km close to the anomaly. Long period mismatches are apparent in the TE mode, however, at sites  $y = 117.3$ , 135.3 and 155.2 km to the left of the anomaly. Large error bars at long periods, particularly in the TM mode, partly account for these discrepancies, but we have also found (see the discussion in Section 3) that the responses at long periods are not entirely insensitive to the vertical extent of the TOBE anomaly and may give less of a mismatch at longer periods if its thickness is somewhat reduced. An application of the Spearman test yielded the  $D$  probabilities 0.37 and 0.24 for the TE and TM responses respectively, again providing no evidence of a systematic trend in the fitting of the response curves.

### 3. Discussion

The Phanerozoic sedimentary layer stretching across the surface of the entire region is well resolved in Figs. 2(b) and 5(c). It has an average resistivity of about  $3 \Omega\text{m}$ , and a thickness of 2.8 km over the NACP anomaly decreasing somewhat to 1.9 km over the TOBE anomaly. A

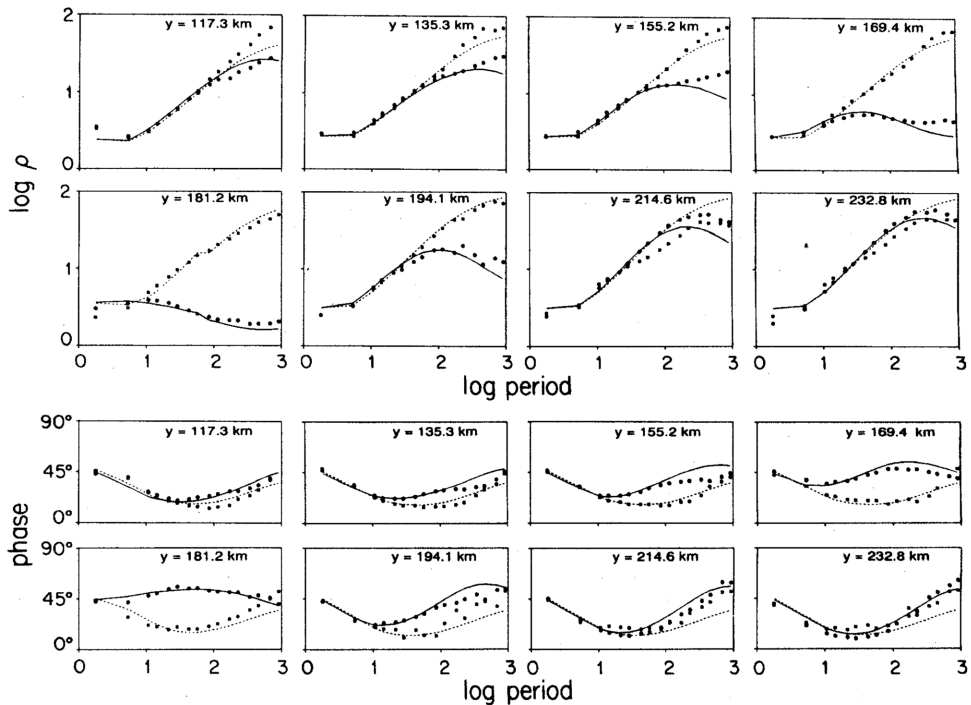


Fig. 6. As in Fig. 3 except that the response curves are for the 5 column model in Fig. 5(c) at the 8 sites traversing the TOBE anomaly.

thinning of the sediments from west to east is in accordance with the observations of JONES and CRAVEN (1990) and the pseudosections of one-dimensional inversions compiled by CONSTABLE *et al.* (1987), as well as by AGARWAL *et al.* (1993).

Our final model of the NACP anomaly itself has been discussed in detail by AGARWAL *et al.* (1993). It is structurally simpler, less conducting, thicker, and dropping only slightly from east to west compared with the model proposed by JONES and CRAVEN (1990) based on pseudosections compiled from the results of one-dimensional OCCAM inversions and trial-and-error modelling. Both blocks necessarily extend right down to the basement because the 1D starting model did not provide enough layers to resolve the presence or otherwise of different material. Below 20 km, the lower crust east of the anomaly is much more conducting than that to the west. Note that the large vertical extent of the anomaly in our model contradicts the assertion of JONES and CRAVEN (1990) that the anomaly cannot be more than a few kilometers in thickness because the TM responses are insensitive to it. It appears from Fig. 3, however, that the TM responses are relatively unaffected by the anomaly, as implied by the observations. As reported in AGARWAL *et al.* (1993) this point was further checked by horizontally dividing the two blocks forming the anomaly in half while leaving their resistivities unchanged. The new model represented exactly the same geo-electric structure but introduced 4 new adjustable parameters (2 horizontal boundaries and 2 resistivities) which gave the anomaly the freedom to shrink to a thin structure as a result of the horizontal boundaries rising and the resistivity of the lower portions of the divided blocks increasing, if that were indeed the correct path to follow towards a global minimum. In fact

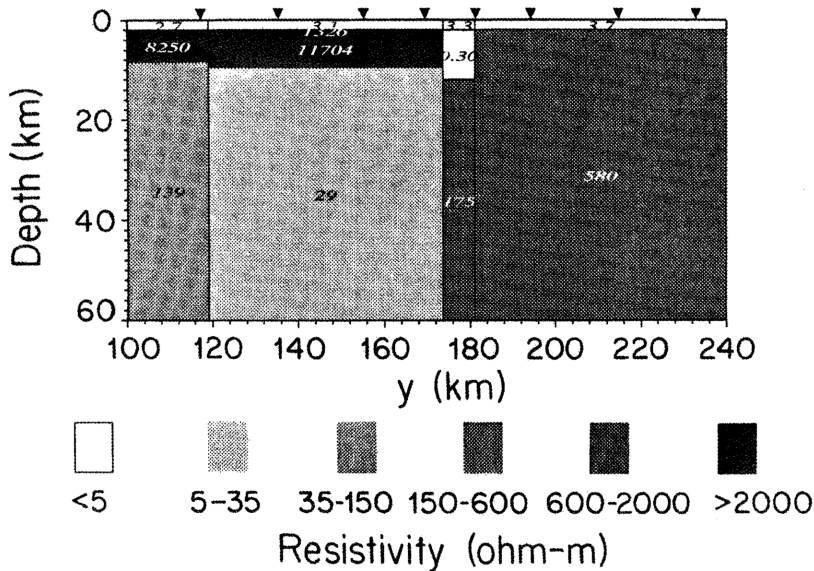


Fig. 7. A thin, electrically isolated model of the TOBE anomaly obtained by manual adjustment of the 'least-blocked' model in Fig. 5(c). The vertical extent of the anomaly in the third column is 10 km and the resistivity of the underlying layer is 175  $\Omega\text{m}$ . Otherwise all parameters are same as in the 'least-blocked' model. The misfit value is  $s^2 = 1.98 \times 10^{-3}$ .

further minimization of the misfit caused virtually no change; the upper section of the wider and taller block on the right of the anomaly did shrink to a thin layer only 6.6 km thick, but since the underlying part of the block with a resistivity of 8  $\Omega\text{m}$  was still more conductive than the rest of the NACP anomaly the new thin layer (whose resistivity was 3  $\Omega\text{m}$ ) could not be considered isolated from the remaining thick conductive blocks in the structure. Moreover the new misfit value of  $s^2 = 1.22 \times 10^{-3}$  was not significantly different from that for the 'least-blocked' model in Fig. 2(b). It is concluded that thick structures are not necessarily excluded from the class of possible models representing the NACP anomaly.

A similar test involving the addition of an extra column was also carried out by AGARWAL *et al.* (1993) with the purpose of ascertaining whether the structure should really slope more steeply westwards as proposed by JONES and CRAVEN (1990). Once again the outcome was not convincing; the new column on the right of the anomaly did rise about 3 km above the main body but it was very narrow and the new misfit value of  $s^2 = 1.20 \times 10^{-3}$  again failed to pass an *F*-test for significance at the 95% confidence level.

The final model of the region around the TOBE anomaly depicted in Fig. 5(c) is also very simple having been reduced to effectively 7 distinct regions. The anomaly itself is highly conductive with a resistivity of 0.3  $\Omega\text{m}$  and is confined in lateral extent to only 7.4 km. While its top reaches to the same level as the base of the sedimentary layer, the two may not be joined electrically because, as mentioned earlier, our inversion scheme automatically eliminated the layer between them once the minimization routine attempted to make it less than 0.5 km thick. The existence of 300–500 m of resistive material between the base of the Phanerozoic and the top of the anomaly (JONES and SAVAGE, 1986) cannot be ruled out—it simply is beyond the capability of our modelling program to resolve without introducing an excessive number of grid points. Nev-

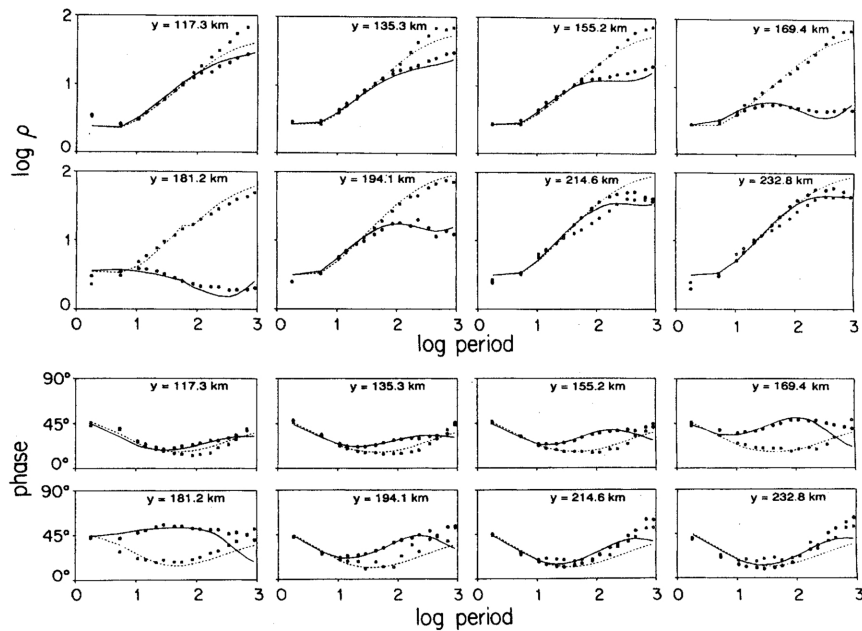


Fig. 8. As in Fig. 6 except the response curves are for the model shown in Fig. 7.

ertheless it is interesting to note that only in the 'least-blocked' model was the intervening layer compressed to such an extent; all the other models in Fig. 5 retained a resistive layer between the sedimentary cover and the anomaly. Otherwise our model includes features similar to those presented by other authors. RANKIN and KAO (1978) first identified the anomaly and concluded that the top of the structure was at a depth of 2.4 km; JONES and SAVAGE (1986) surmised from modelling studies that it was narrower and more vertical than the NACP anomaly and at a depth of 2.1 km; and according to their colour-coded pseudosection JONES and CRAVEN (1990) deduced from one-dimensional inversions a resistivity of less than  $1 \Omega\text{m}$  for the central part of the TOBE anomaly.

A feature of the final model, alluded to in Section 2, is the presence of the 1 km thick layer at the base of the third column from the left. Its resistivity (not shown in the figure) is  $6.8 \Omega\text{m}$ . The fact that it remained there supports the conclusion that the TOBE anomaly is indeed the thin, vertically extended structure shown, for otherwise the bottom layer boundary would surely have been raised during optimization. Nevertheless, we have explored this question further because it is difficult to resolve the vertical extent of structures with MT data alone in the presence of the screening effect provided by a surface layer of conductive sediments, and it is always possible that the minimization routine settled into a false local minimum when the true global minimum demanded a much less elongated anomaly. Our procedure was to raise artificially the bottom layer boundary in the third column to 7 different levels keeping all other parameters fixed, and then calculating the new misfit values in each case. The various levels were chosen such that the vertical thickness of the TOBE anomaly decreased from 57 km to successively 45, 35, 25, 15, 10, 8.5, and 5.0 km. It was found that the misfit increased only slightly to  $s^2 = 2.00 \times 10^{-3}$  as the thickness of the anomalous block was reduced to 10 km, but thereafter became progressively worse. Such a small and barely significant change in misfit over quite a large range of thicknesses

suggests that the TOBE anomaly could indeed be modelled adequately with a much less elongated structure (as little as 10 km) than that shown in Fig. 5(c). A further numerical experiment was carried out on the modified model in which the resistivity of the layer beneath the anomaly of 10 km thickness was changed from  $6.8 \Omega\text{m}$  to a series of larger values—50, 175, 500, and 2000  $\Omega\text{m}$ —and the new misfit calculated each time. The results of this test showed that it mattered little how effectively the thin anomaly was insulated electrically from the underlying region. The misfit varied only slightly the best value being  $s^2 = 1.98 \times 10^{-3}$  when the resistivity beneath the anomaly was 175  $\Omega\text{m}$ . Similar experiments with different anomaly thicknesses gave essentially the same results. Note that none of the new misfit values obtained for these manually adjusted models were smaller than the value of  $1.82 \times 10^{-3}$  for the 'least-blocked' model, although some of them were not sufficiently greater as to be rejected out of hand.

In Fig. 7 we have reproduced one such 'manually adjusted' model—the one with a 10 km thick anomaly, and an underlying resistivity of 175  $\Omega\text{m}$ , and a comparison of its TE and TM apparent resistivity and phase responses with those observed is shown in Fig. 8. One difference between the responses for this model and those for the 'least-blocked' model in Fig. 5(c) occurs in the TE phases at sites  $y = 169.4, 181.2$  and  $194.1$  km which now tend to be smaller than the actual responses whereas they were somewhat larger for the 'least-blocked' model. Another is in the long period apparent resistivity curves which pick up the increased resistivity at depth under the anomaly in Fig. 8.

#### 4. Conclusions

Our method of seeking a 'least-blocked' model provides a rather different approach to two-dimensional inversion of MT data from the usual methods in which the model is over-parameterized and a best-fitting solution is sought subject to some regularizing condition such as a maximum smoothness constraint. It is very computer intensive and depends for its successful implementation on the availability of a powerful workstation allocated solely to this task. The development of the method as a practical alternative only became possible when an efficient forward modelling program which designed its own numerical grids automatically became available.

While the method has delivered models of the NACP and TOBE anomalies beneath a surface sedimentary layer which contain many of the features proposed by other authors using different types of inversion schemes, there are some notable differences which are characteristic of our approach. Thus we have found a two-block model of the NACP anomaly which extends to a greater depth than the thin layer models proposed by other authors and the TOBE anomaly is found to be similarly elongated in the vertical direction but much thinner horizontally and more conductive than the NACP anomaly. It was found by manual adjustment of the TOBE model that a less thick structure underlain by a resistive host also gave an acceptable misfit value and response curves that appeared to match the data as adequately as the response of the 'least-blocked' model. However, no such manual adjustment of the NACP model was as successful; the thick conductive structure extending to the basement appears to be an essential feature of our NACP model which cannot be modified without causing a deterioration in the fit of the response curves.

The Williston Basin (COPROD2) data were kindly made available to the Geological Survey of Canada, Ottawa by P. J. Savage of PanCanadian Petroleum Ltd., Calgary, Alberta. The authors wish to thank Alan Jones of the Geological Survey for supplying us with the data corrected for static shift. This work is supported by research grants from the Natural Sciences and Engineering Research Council of Canada and the University of Victoria.

## REFERENCES

- AGARWAL, A. K., H. E. POLL, and J. T. WEAVER, One and two dimensional inversions of MT data in continental regions, *Phys. Earth Planet. Inter., Hutton Symposium issue*, 1993 (in press).
- BEVINGTON, P. R., *Data Reduction and Error Analysis for the Physical Sciences*, McGraw-Hill, New York, 1969.
- CONSTABLE, S. C., R. L. PARKER, and C. G. CONSTABLE, Occam's inversion: a practical algorithm for generating smooth models from EM sounding data, *Geophysics*, **52**, 289–300, 1987.
- DEGROOT-HEDLIN, C. D. and S. C. CONSTABLE, Occam's inversion to generate smooth, two-dimensional models from magnetotelluric data, *Geophysics*, **55**, 1613–1624, 1990.
- FISCHER, G. and B. V. LEQUANG, Topography and minimization of the standard deviation in one-dimensional magnetotelluric modelling, *Geophys. J. R. astr. Soc.*, **67**, 279–292, 1981.
- JONES, A. G., The COPROD2 dataset: Tectonic setting, recorded MT data and comparison of models, *J. Geomag. Geoelectr.*, this issue, 933–955, 1993.
- JONES, A. G. and J. A. CRAVEN, The North American Central Plains conductivity anomaly and its correlation with gravity, magnetic, seismic, and heat flow data in Saskatchewan, Canada, *Phys. Earth Planet. Inter.*, **63**, 169–194, 1990.
- JONES, A. G. and P. J. SAVAGE, North American Central Plains conductivity anomaly goes east, *Geophys. Res. Lett.*, **13**, 685–688, 1986.
- PEDERSEN, L. B. and T. M. RASMUSSEN, Inversion of magnetotelluric data: a non-linear least-squares approach, *Geophys. Prospect.*, **37**, 669–695, 1989.
- PRESS, W. H., B. P. FLANNERY, S. A. TEUKOLSKY, and W. T. VETTERLING, *Numerical Recipes*, Cambridge University Press, Cambridge, 1989.
- RANKIN, D. and D. KAO, The delineation of the Superior-Churchill transition zone in the Canadian shield, *Can. Soc. Explor. Geophys.*, **14**, 50–54, 1978.
- SMITH, J. T. and J. R. BOOKER, Magnetotelluric inversion for minimum structure, *Geophysics*, **53**, 1565–1576, 1988.
- WEAVER, J. T. and A. K. AGARWAL, Automatic one-dimensional inversion of magnetotelluric data by the method of modelling, *Geophys. J. Int.*, **112**, 115–123, 1993.